JOURNAL OF MATERIALS SCIENCE **34** (1999) 4821 – 4830

An electron microscopy study of the formation of hydroxyapatite through sol-gel processing

A. JILLAVENKATESA, D. T. HOELZER, R. A. CONDRATE, SR.
New York State College of Ceramics, Alfred University, Alfred, NY 14802

A study of the stages involved in the formation of hydroxyapatite synthesized by a sol-gel route was performed using scanning and transmission electron microscopic techniques as the primary characterization tools. Scanning electron microscopy enabled examination of the samples of the gel heat treated at various temperatures and for different time periods to determine the morphology and size of grains along with the presence and extent of any porosity in the sample surfaces. Thus, phase development could be studied as a function of heat treatment time and temperature. The gel was prepared using calcium acetate and triethyl phosphate as precursors added in a Ca/P molar ratio of 1.67. Characterization of the samples using transmission electron microscopy allowed a closer examination of the interaction between individual particles and also the detection of features on a much finer scale. Results deduced from these techniques were compared with those obtained from X-ray diffraction and FTIR spectroscopy.

1. Introduction

Numerous ceramic materials have been finding increasing acceptance in the biological field [1–3] for a wide range of applications. Hydroxyapatite ($Ca_{10}(PO_4)_6(OH)_2$) belongs to this class of materials that are being used for orthopedic and oral/ maxillofacial implants and surgery [4, 5]. Hydroxyapatite is a calcium phosphate-based material that has a chemical composition similar to the calcified/mineral part of human bone. This chemical similarity with the aid of appropriate porosity and crystallinity [6–8] permits direct chemical bonding between the bone and the hydroxyapatite surface. The non-toxic nature and biocompatibility of hydroxyapatite [9, 10] has thus made it a material subject to extensive research with regards to synthesis, characterization and applications.

Numerous techniques for synthesis and development of apatites have been developed over the years. Amongst the earliest techniques reported, was a technique involving the hot-pressing of fluoroapatite ($Ca_{10}(PO_4)_6F_2$, a naturally occurring mineral) to form a solid bar under pressures of approximately 5000 psi and temperatures of 920–1230 °C by Levitt *et al*. [11]. Hydrothermal techniques have also been applied to prepare hydroxyapatite using "porites corals" from the Cuban Sea as per the reaction [12]:

$$6(NH_4)_2HPO_4 + 10CaCO_3 + 2H_2O \rightarrow Ca_{10}(PO_4)_6(OH)_2 + 6(NH_4)_2CO_3 + 4H_2CO_3.$$

The most widely used techniques of synthesis are however based on precipitation routes. These routes involve precipitation reactions between suitable calcium and phosphate precursors under very tightly controlled pH conditions, leading to the formation of hydroxyapatite seed crystals. These crystals are then sintered at elevated temperatures in the range of 1000–1200 °C to produce dense polycrystalline hydroxyapatite. An example of applying this technique has been reported by Jarcho *et al*. [13] who precipitated hydroxyapatite at a pH of 11–12 by the following reaction:

$$10Ca(NO_3)_2 + 6(NH_4)_2HPO_4 + 2NH_4OH \rightarrow \text{Hydroxyapatite}.$$

A major problem encountered in this technique is the decomposition of hydroxyapatite to tricalcium phosphate ($Ca_3(PO_4)_2$) and tetracalcium phosphate ($Ca_4P_2O_9$) at the sintering temperature as per the reaction:

$$Ca_{10}(PO_4)_6(OH)_2 \rightarrow Ca_3(PO_4)_2 + Ca_4P_2O_9 + H_2O.$$

This problem has been overcome by techniques involving the hydrolysis of hydroxyapatite at lower temperatures in an aqueous medium under pH range of 9.5–10.5 [14]. Often, in these latter techniques, formation of hydroxyapatite is accompanied by the formation of a second phase, comprising of calcium deficient hydroxyapatite. Sol-gel routes to develop hydroxyapatite have also been of much interest, due to the advantages gained by this technique. Deptula *et al*. [15] have reported a modification of the sol-gel technique involving a repetitive process of emulsification of a mixture of calcium acetate and phosphoric acid followed by the solidification of the emulsion by water extraction and calcination to form hydroxyapatite. Various authors have reported developing thin films of hydroxyapatite by the sol-gel

route using different calcium and phosphate precursors [16, 17]. The present authors have also reported a technique to develop hydroxyapatite using calcium acetate and triethyl phosphate as precursors with suitable alkyl additives to help in the formation of the colloidal gel [18].

Due to the complex nature of the sol-gel techniques, characterization of the products formed at various stages of processing is of extreme interest to identify and interpret the processing stages. This study uses scanning and transmission electron microscopy as primary tools, with the aid of X-ray diffraction techniques and FTIR spectroscopy to follow the development of the hydroxyapatite phase in powders synthesized using a sol-gel route. The application of electron microscopic techniques enables characterization of features such as the morphology of the powders, presence and extent of external pores, orientation and placement of grains through lattice patterns (Moiré fringes) and positive identification of the sample through features such as electron diffraction patterns. Contrast developed by the passage of electrons through the thin sections of the sample in transmission electron microscopy is of particular help in studying the internal characteristics of the sample.

2. Experimental

2.1. Sol-gel processing

The sol-gel processing route for preparation of hydroxyapatite followed in this study involved the addition of 0.012 mol of triethyl phosphate* ($PO(OC_2H_5)_3$) to 0.02 mol of calcium acetate† ($Ca(C_2H_3O_2)_2$) to maintain a Ca/P molar ratio of 1.67, as is found in stoichiometric hydroxyapatite. Four different batches were set up, with one batch containing only the calcium and phosphate precursors and the other three batches also containing either 5 ml of methanol, 5 ml of ethanol or 5 ml of propanol each. Measuring and mixing of all chemicals was done in a controlled environment chamber where relative humidity of the chamber was maintained below 50%. The batches were covered and placed on a magnetic stirrer and the sols were stirred vigorously for 12 h at 25–30 °C, followed by stirring at 40–45 °C for 12 h. The temperature was then raised to 75 °C, and sample batches were held at that temperature for 10 h. After gelation, the gels were dried at 120 °C for 10 h in air. The resultant gels were ground to a fine powder (finer than 200 μm) and heat treated at temperatures ranging from 400 °C to 1200 °C in air. The heat treatment temperatures were determined from the differential thermal analysis (DTA) and thermogravimetric analysis (TGA) curves for the gel obtained upon heating the gel from room temperature to 1200 °C at a heating rate of 10 °C/min. The powders were then characterized by X-ray diffraction for phase identification and FTIR spectroscopy for structural content. Samples for transmission electron microscopic studies were heat treated at 900, 950, 1000 and 1100 °C for different time periods as explained in the results and discussion section. Samples heat treated at 900 °C and above were stirred in a 0.01M HCl solution for 2 h to convert the CaO present in the samples to $CaCl_2$, which was, washed away with distilled water by filtration through a Whatman 42 filter paper. The residue after filtration was dried at 120 °C to obtain the hydroxyapatite phase.

2.2. Electron microscopic characterization

Transmission electron microscopic studies of the samples were performed on a Jeol‡ JEM 2000FX instrument. Sample specimens were prepared by dispersing the powders in distilled water to form very dilute suspensions and then dropping a few droplets on copper grids with carbon coated formvar film supports. The grid was then dried out to remove any moisture leaving only extremely fine sample particles on the grid for analysis. Care was taken to avoid deposition of large, thick clusters of powders to permit transmission of the electron beam through the sample. The powder samples were studied under an electron beam accelerated by a potential of 120 keV.

The powder specimens for scanning electron microscopy were prepared by ultrasonic dispersion of the powders in distilled water. A few drops of the suspension were pipetted onto a carbon stub that was mounted on a standard SEM stub with conducting silver paste. The sample stubs were dried, and the samples were sputter coated with an approximately 10 nm thick Au-Pd coating. The samples were then studied with an Amray§ 1810 SEM. Samples were examined under an electron beam with an acceleration potential varying between 14–16 keV.

2.3. X-Ray diffraction and FTIR spectroscopic characterization

Samples were characterized by X-ray diffraction on a Kristalloflex 810¶ X-ray diffractometer. Samples were studied by X-ray beams of 0.15412 nm wavelength, generated from a copper target under an acceleration potential of 40 kV and beam current of 30 mA. FTIR spectroscopic studies were performed on a Nicolet* 60SX mid-IR spectrometer. All samples were studied in the transmission mode with the samples being made by mixing 1 mg of sample powder with 300 mg of KBr and pressing the mixture under a pressure of 1200 psi to form a pellet. The spectrometer was set to a spectral resolution of 4.0 cm^{-1}.

3. Results and discussion

The formation of hydroxyapatite by the sol-gel route described above has been established and discussed in considerable detail by the present authors in a previous study [18]. It was shown that hydroxyapatite

*Fluka Chemicals, Ronkonkoma, NY.
†Sigma Chemical Corp., St. Louis, MO.
‡JEOL, Peabody, MA.
§Amray Inc., Bedford, MA.
¶Siemens, Munich, Germany.
*Nicolet Instruments Corp., Madison, WI.

was formed in all of the four sample batches upon heat treatment of the dried gels. The results and discussion reported here appertain to the characterization of the formation of hydroxyapatite and other phases by electron microscopic techniques.

3.1. Thermal analyses of dried gels

The gels formed by the sol-gel route described above, after drying were subject to thermal analysis using differential thermal analysis (DTA) and thermogravimetric analysis (TGA). The results of the differential thermal analyses of the four sample batches are illustrated in Fig. 1. As can be seen, there are no considerable differences in the nature and occurrence temperatures of the endothermic and exothermic peaks observed in the four batches. Fig. 2 illustrates the differential thermal analysis trace together with the thermogravimetric analysis trace of the sample batch with no alcohol additive in detail. In this figure, three endothermic regions

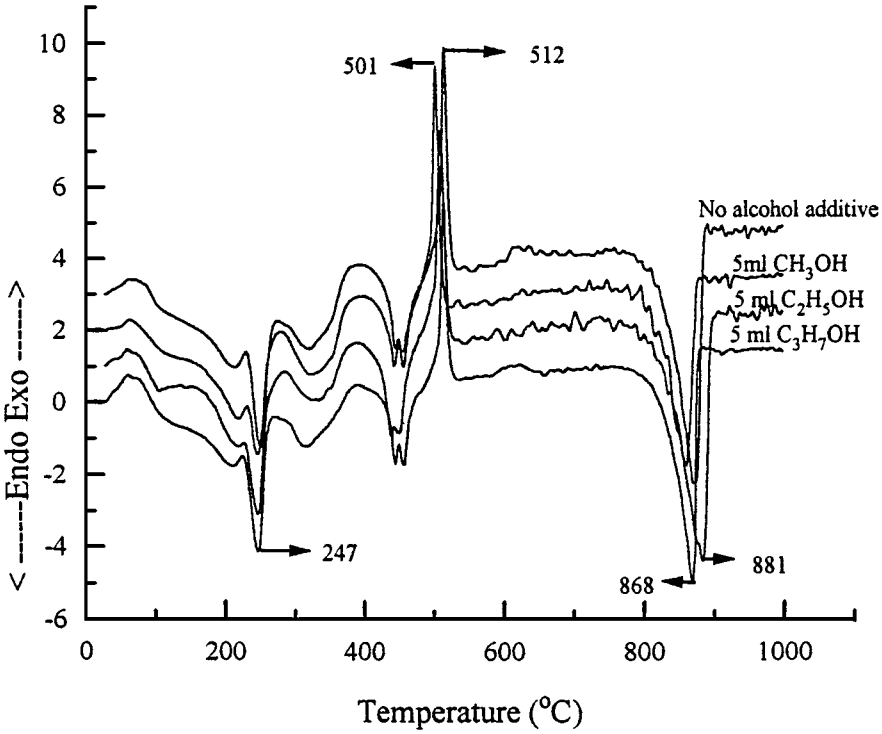

Figure 1 Differential Thermal Analysis traces of gels prepared by the sol-gel route with different alcohol additives.

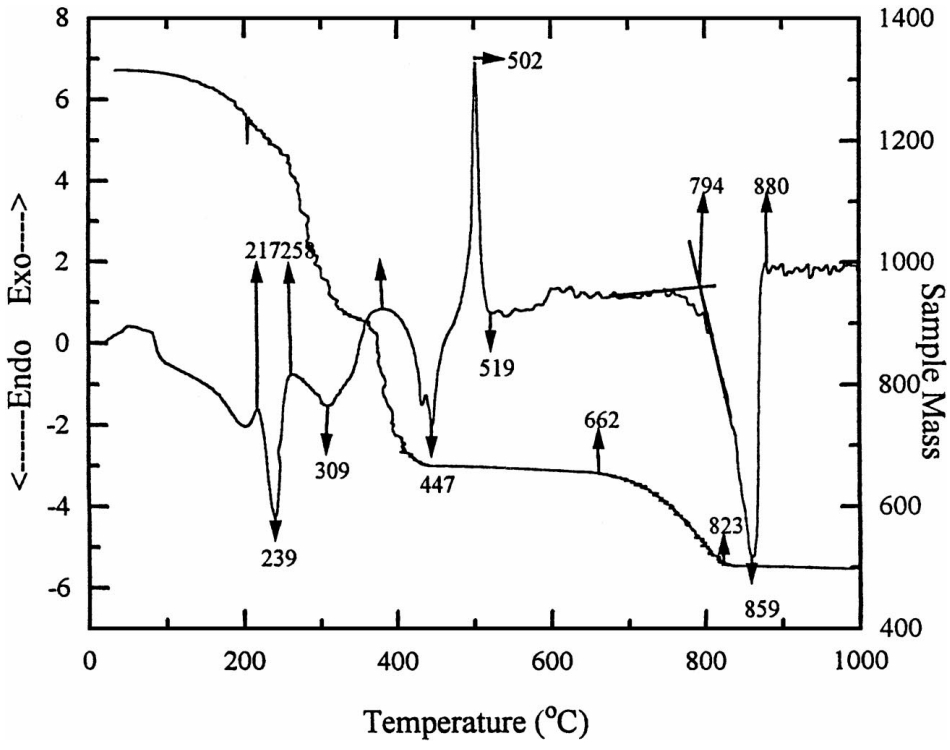

Figure 2 DTA/TGA trace of gel with no alcohol additive heated from room temperature to 1000 °C, at a heating rate of 10 °C/min.

in the temperature range of about 200–450 °C are discerned. Together with the TGA trace, which indicates a significant loss in sample mass in this temperature regime, one can conclude that these endothermic regions centered at 239, 309 and 447 °C correspond to the evolution of organic compounds formed due to reactions between the precursors added to create the sol. The strong exothermic peak at 502 °C is representative of the exothermic reaction indicating the formation of hydroxyapatite. However, the sample batches at this stage consist of hydroxyapatite in the very early stages of crystallization and calcium carbonate as calcite, which was formed due to the interaction between the evolved organics and the extremely reactive calcium present in the gel. Further heating is necessary to cause the development and enhanced maturation of the crystallized hydroxyapatite. Upon reaching a temperature of approximately 800 °C, the onset of the endothermic peak seen in the DTA trace in Fig. 2, indicates the breakdown of calcium carbonate present in the system to form calcium oxide accompanied by the evolution of CO_2. These stages of phase evolution have been characterized using X-ray diffraction techniques, and the results are illustrated in Fig. 3 showing the X-ray diffraction patterns of the gel obtained from the batch with no alcohol additive heat treated at different temperatures.

3.2. Elimination of calcium oxide

The HCl treatment as described in the experimental procedures is necessary to eliminate the CaO from the CaO and hydroxyapatite mixture obtained upon heat treating the gel at temperatures above 900 °C. CaO is converted to $CaCl_2$ and due to its significantly higher solubility in water, as compared to the relatively negligible solubility of hydroxyapatite in water, the $CaCl_2$ is eliminated from the system. The hydroxyapatite is reclaimed as a residue by filtering the HCl solution. The residue is then dried at 120 °C for 2 h. Fig. 3b indicates the X-ray diffraction patterns for the sol-gel batch heat treated at 1000 °C, prior to and post to the HCl treatment, showing the elimination of calcium oxide. The elimination of calcium oxide phase and residual organics, as followed using FTIR spectroscopy, is illustrated in Fig. 4b.

With the development of hydroxyapatite thus established, samples heat treated at various temperatures were examined using scanning electron microscopy. Small batches of the gel with no alcohol additives were heat treated at 460, 550, 775, 900, 1000, 1100 and finally at 1200 °C. The samples were held at these temperatures for 10 h and then air quenched to room temperature. The samples were characterized using X-ray diffraction and FTIR spectroscopies to identify the phases formed, and then were examined by scanning electron microscopy. Hydroxyapatite powder samples from the other sol-gel batches (i.e. batches containing varying R–OH, where, R = methyl, ethyl and propyl) obtained by heat treatment at 1000 °C, followed by the HCl wash were examined to determine if any differences in the morphology could be discerned using SEM techniques.

3.3. HA phase development as a function of heat treatment temperature

Fig. 5a–i represents the SEM images of the sample batch with no alcohol at different stages of heat treatment. An image of the powder obtained from the sample heat treated at 460 °C is seen in Fig. 5a. This image shows a large monolith with a very rough surface. The rough surface of this monolith can be related to pores formed by the evolution of organics in the form of gases at lower temperatures. From the X-ray diffraction patterns, it is known that at this temperature, the sample consists predominantly of calcium carbonate and some amorphous phases. Upon heating to 550 °C (a temperature above the exotherm indicating the formation of hydroxyapatite), we see from Fig. 5b some very small grain morphology which is approximately 200 nm in diameter formed on the surface of the monolith similar to that observed in Fig. 5a. The random presence and small size of these grains indicates a possible nucleation and growth mechanism responsible for creating these grains. Fig. 5c represents the image of a sample heat treated at 775 °C. The image shows an increase in the number of these small grains first observed upon heating the sample at 550 °C. Also, the grain size of the first nucleated grains is seen to be significantly larger with the grain diameter being close to 700–800 nm. Other similar grains with much smaller dimensions are observed on the surface of the monolith. The surface texture of the monolith shows a very coarse nature, and may be due to the possible evolution of CO_2 from the interior of the monolith. Upon heating to 900 °C (a temperature past the endotherm due to decomposition of calcium carbonate to calcium oxide and carbon dioxide), we see the small grains starting to form clusters on a large basal substrate (see Fig. 5d). These cluster sizes are observed to range in size from about 500 nm to 2 μm in diameter. The individual grains forming these clusters are observed to be about 200 nm in diameter. From the increasing quantity of observed grains with increasing heat treatment temperatures one may now assume that these small grains are the hydroxyapatite phase. As can be expected, heating the sample at 1000 °C leads into the early stages of sintering of the sample. This leads to grain coarsening, and the increased temperatures induce further crystallization of grain leading to a drastic increase in the number of grains that are observed. The individual grains are almost equiaxed with no perceptible preferred axis of growth, and having a grain size of about 500 nm in diameter. Fig. 5e illustrates a cluster of such grains observed at a magnification of 7300×. Examination of a similar cluster at a greater magnification of 14,700× (see Fig. 5f) indicates that the grains start to develop a hexagonal shape consistent with the hexagonal space group in which the unit cell crystallizes. The clusters show extensive macroporosity while the individual grains are observed to be free of any surface pores.

At this point of phase development, characterization of the sample indicates the existence of calcium oxide, together with hydroxyapatite. Calcium oxide is eliminated from the system by conversion to calcium chloride and is then dissolved in distilled water using HCl.

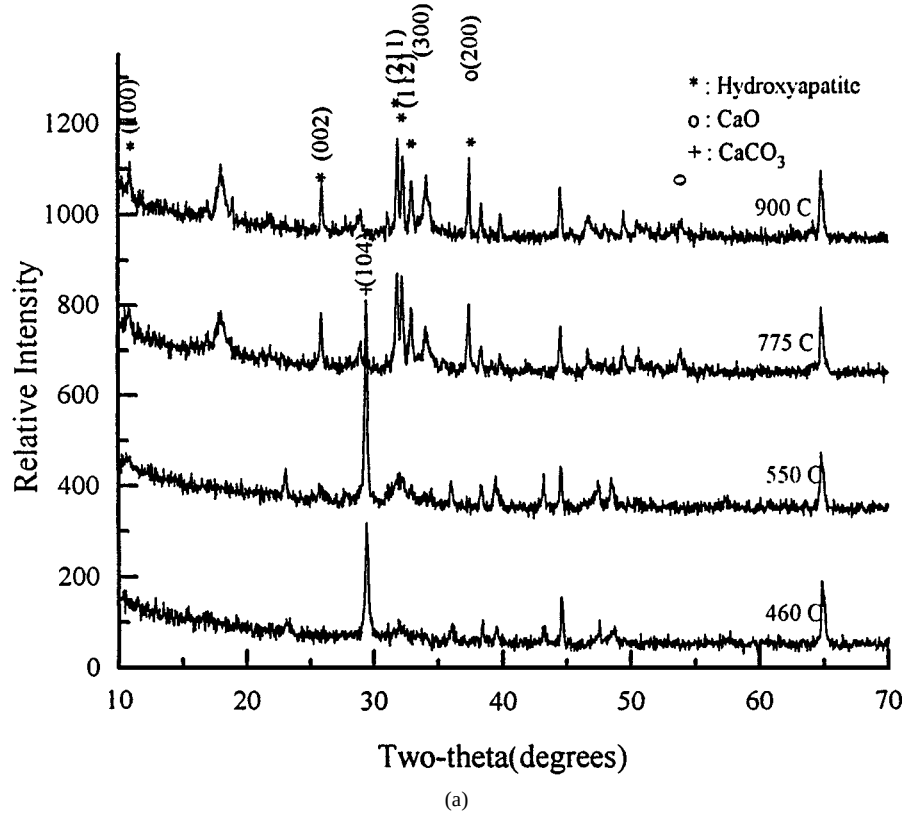

(a)

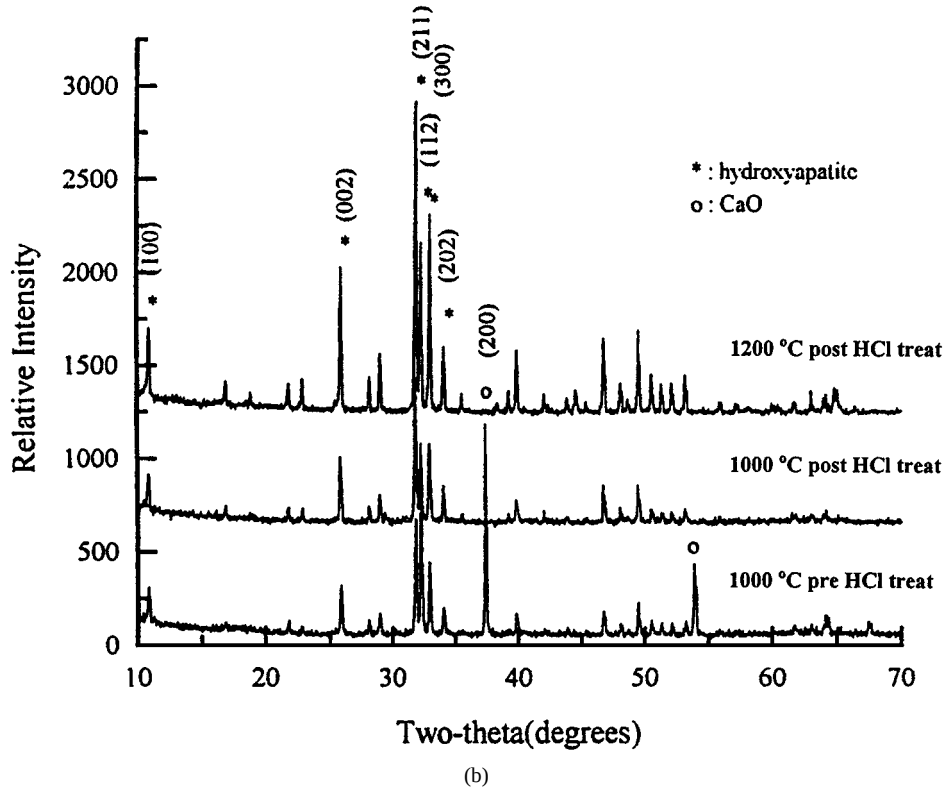

(b)

Figure 3 (a) X-ray diffraction patterns for gel with no alcohol additive heat treated at 460, 550, 775 and 900 °C and (b) X-ray diffraction patterns for gel with no additive heat treated at 1000 °C prior to and post HCl treatment and at 1200 °C post HCl treatment.

The resultant residue is observed to consist of hydroxyapatite. No significant differences are observed in the SEM images of the sample prior to and post to HCl treatment. Fig. 5g shows the image of the sample after the HCl treatment. As is observed from this image, the grains show morphological characteristics very similar to those observed in Fig. 5e and f. No changes in the grain size and shapes are observed after the HCl treatment, thereby providing proof that these grains are not due the calcium oxide and are thus of hydroxyapatite, by default.

Heat-treatment of the sample at temperatures above 1000 °C leads to further sintering and subsequent coarsening of the grains. The powder sample heat treated at

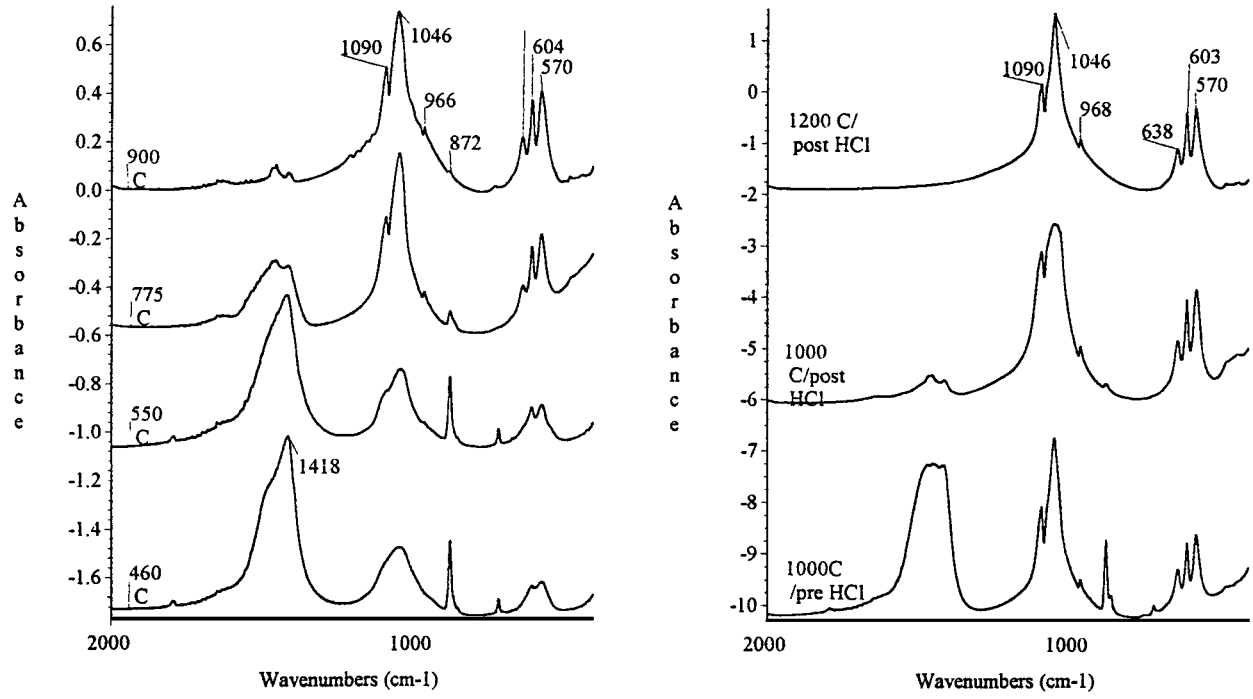

(a) (b)

Figure 4 (a) FTIR spectra of gel with no alcohol additive heat treated at 460, 550, 775 and 900 °C and (b) FTIR spectra of gel with no alcohol additive heat treated at 1000 °C prior to and post HCl treatment and at 1200 °C post HCl treatment.

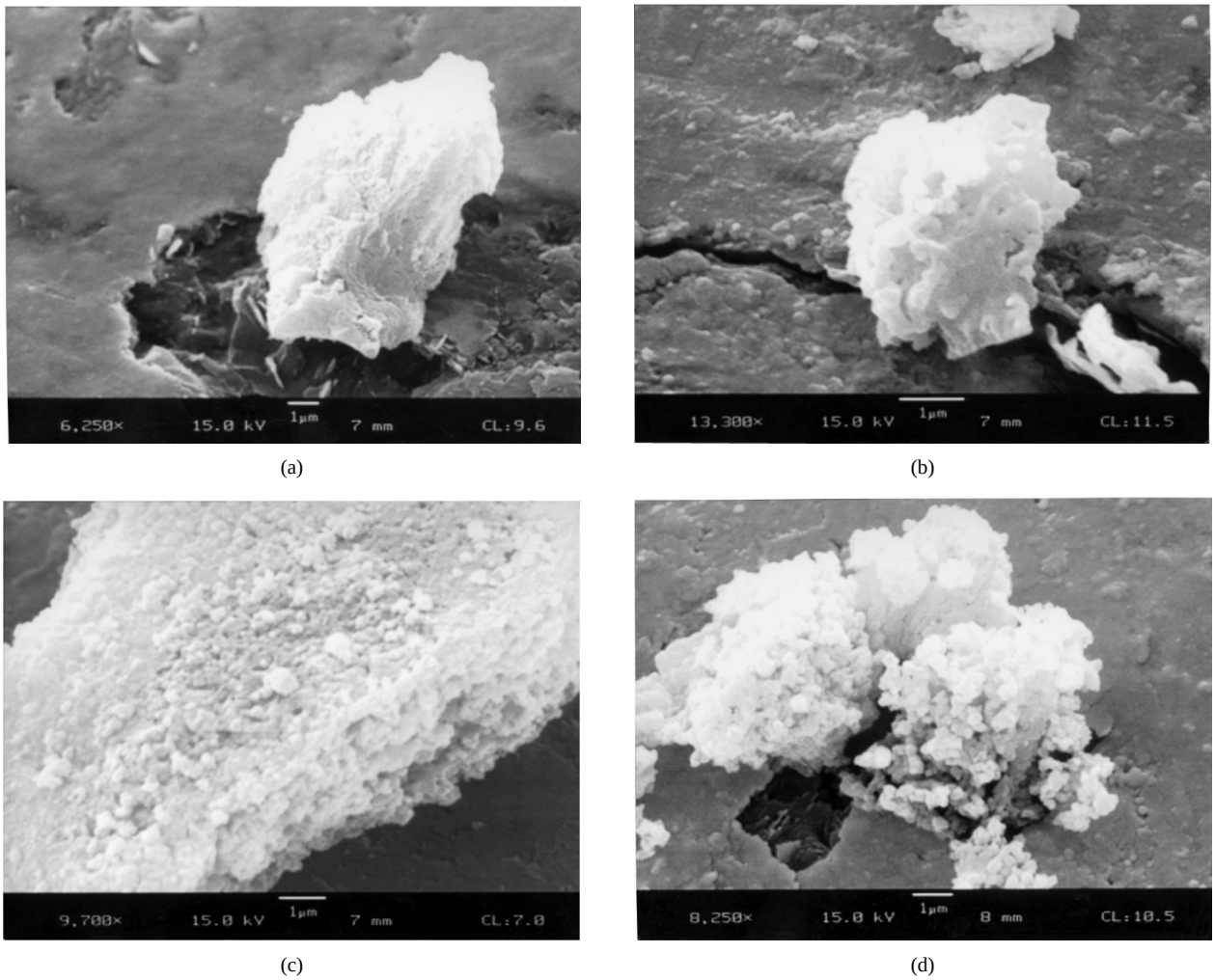

(a) (b)

(c) (d)

Figure 5 (a) SEM image of gel heat treated at 460 °C, (b) SEM image of gel heat treated at 550 °C, (c) SEM image of gel heat treated at 775 °C, (d) SEM image of gel heat treated at 900 °C, (e) SEM image of gel heat treated at 1000 °C prior to HCl treatment, (f) SEM image of gel heat treated at 1000 °C prior to HCl treatment, (g) SEM image of gel heat treated at 1000 °C post HCl treatment, (h) SEM image of gel heat treated at 1100 °C post HCl treatment, and (i) SEM image of gel heat treated at 1200 °C post HCl treatment. (*Continued*)

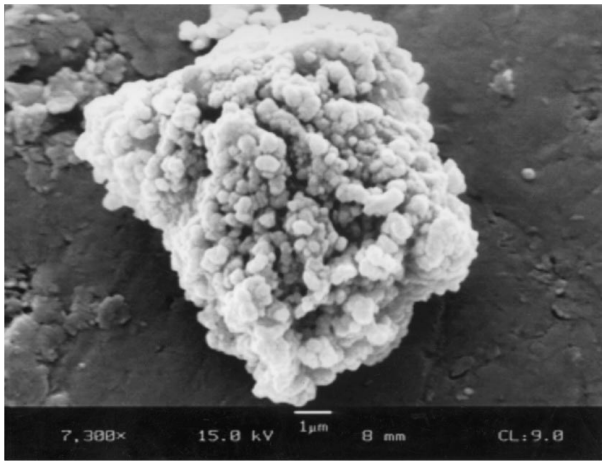

(e)

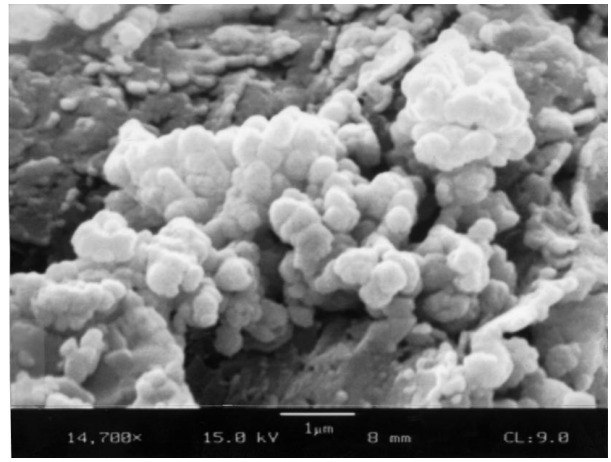

(f)

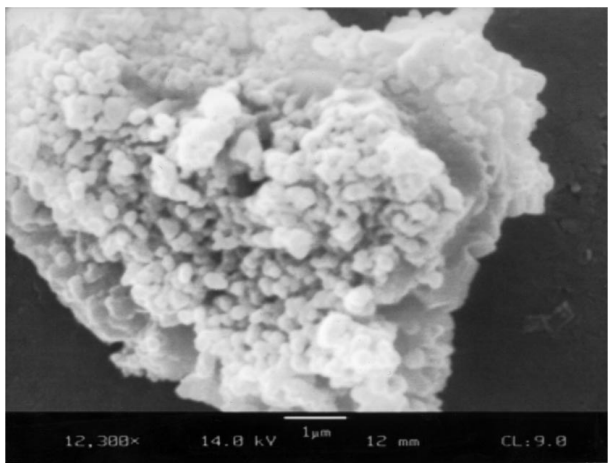

(g)

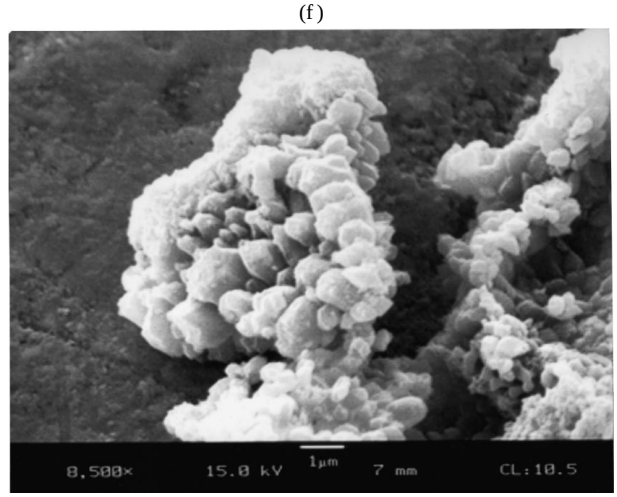

(h)

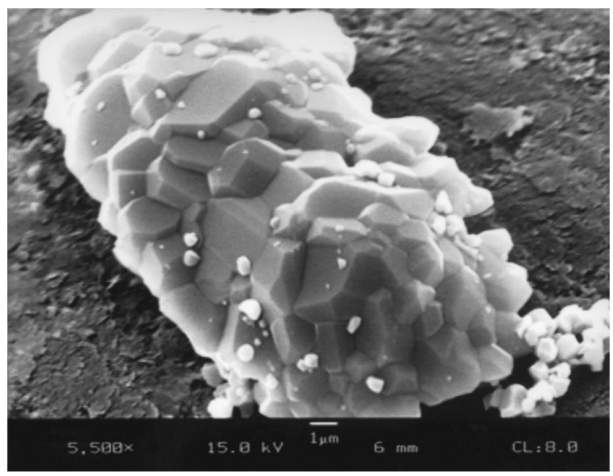

(i)

Figure 5 (*Continued*).

1100 °C, followed by the HCl treatment shows an enhancement in the grain morphology (see Fig. 5h) causing the grains to develop a more pronounced hexagonal shape. Preferential grain growth is also observed so that some grains are observed to have a grain diameter of about 1 μm while other grains with diameter of about 500 nm are observed in the vicinity of these larger grains. The hydroxyapatite grains observed at 1200 °C show a very pronounced grain growth and development.As is noted in Fig. 5i, large hexagonal grains of about 4–5 μm diameter are observed. These grains appear to be dense with no intragranular porosity. Some small grains that are less than 1 μm are observed at triple points of the hydroxyapatite grain boundaries and on the surface of the hydroxyapatite grains. These small grains may have been reduced in size due to the preferential exaggerated grain growth of neighboring hydroxyapatite grains.

The X-ray diffraction patterns for the samples studied after heat treatment at different temperatures mirrors the same trend in the development of different phases. As is seen in Fig. 3a, the X-ray diffraction pattern for

the sample at 460 °C is dominated by the peak ascribed to calcium carbonate. At 550 °C along with this peak, peaks corresponding to the formation of hydroxyapatite first begin to appear. At this temperature, the peaks are ill-defined which are indicative of weak scattering from this phase. However, with increasing treatment temperatures, these peaks become more dominant as is evidenced in the pattern of the sample heat treated at 775 °C. A significant increase in the intensity of the peaks characteristic of CaO, relative to the intensity of the peaks of hydroxyapatite indicates an increase in the amount of CaO with increase in the heat treatment temperature to 900 °C. Furthermore, this pattern exhibits the emergence of a new set of peaks characteristic of calcium oxide with the disappearance of the peak corresponding to calcium carbonate, consistent with the decomposition of calcium carbonate to calcium oxide and CO_2. The elimination of calcium oxide is noted in Fig. 3b which shows the X-ray diffraction patterns of the sample heated at 1000 °C, prior to and post to the HCl treatment. Also, no new peaks are observed in the X-ray diffraction patterns of hydroxyapatite synthesized by heat treating the sample at 1200 °C. The corresponding FTIR spectra are shown in Fig. 4a and b. The spectra of the samples heat treated at 460, 550, 775 and 900 °C are shown in Fig. 4a. The spectrum of the sample at 460 °C shows a very poorly defined, broad band in the region where bands due to phosphate ions in the hydroxyapatite should be present. The strong bands observed are at 1418 and 872 cm^{-1} which are representative of vibrations associated with organic compounds (primarily involving CO_3^{2-} ions). An interesting feature to note is the reduction in the intensity of the vibrational bands occurring at ca. 1418 and 872 cm^{-1} upon heat treatment through 900 °C, followed by a reappearance of these bands upon heat treatment at 1000 °C, prior to the HCl treatment. The wavenumber position of the bands indicate the bands to be characteristic of the vibrations of the carbonate ions. The initial reduction in intensity of these bands would be consistent with the breakdown of calcium carbonate and other organic compounds upon heat treatment, to calcium carbonate. As these organic compounds are not entirely eliminated, the incorporation of these into the hydroxyapatite lattice to form hydroxy carbonate apatite (HCA) would lead to the reappearance of the bands upon heat treatment at 1000 °C. The band at ca. 1418 cm^{-1} is characteristic of the ν_{3a} vibration of a B-site substituted CO_3 ion, while that at 872 cm^{-1} is characteristic of the ν_2 normal mode of the B-site substituted CO_3 ion. Simultaneously, with increasing heat treatment temperatures, the bands associated with the vibrations of the PO_4^{3-} ions increase in intensity showing an increase in the relative concentration of the latter species giving rise to these vibrations. These bands are present at 1090 and 1046 cm^{-1} (splitting of the ν_3 fundamental stretching mode of the PO_4^{3-} ion), at 966 cm^{-1} (ν_1 symmetric stretching mode) and at 570 and 604 cm^{-1} (splitting of the ν_4 fundamental bending mode). Upon heat treatment at 1000 °C which is followed by the HCl treatment to eliminate residual CaO, the bands observed in Fig. 4b are due to the hydroxyapatite with possibly a very small quantity of carbonate-hydroxyl apatite giving rise to a band at ca. 1470 cm^{-1}. At 1200 °C, the very large grains create a very intense absorption pattern with only the vibrational bands of hydroxyapatite being observed.

3.4. HA phase development as a function of soaking time

One may note that the observed increase in the number of HA crystals was most obvious in the temperature range of 900–1000 °C, based upon the development of the hydroxyapatite phase observed by the SEM studies and X-ray diffraction. The next stage of this study was to study the development of the hydroxyapatite phase as a function of time and analysis of the resultant samples using transmission electron microscopy. Samples were heat treated at 950 °C for 0.5, 1, 4 and 8 h followed by HCl treatment to eliminate calcium oxide. Samples of the gel were also heat treated at 900 °C for comparison with the sample heat treated at 950 °C.

Fig. 6a shows the TEM image of the sample heat treated at 950 °C for 0.5 h. It is to be expected that due to the very short heat treatment time, the crystallization of hydroxyapatite would be at its very early stages, and the sample would have some residual organic matter. From the corresponding image some coarsely hexagonal shaped grains are observed. These grains are approximately 60–80 nm in diameter. Also, a very fine thin layer of matter is observed along the edges of the specimen. The lack of definite crystals in this region (which was determined by darkfield imaging) indicates possibly an amorphous nature to this region. Increasing the heat treatment time to 1 h at 950 °C causes an increase in the number of crystallized grains (Fig. 6b). These grains vary in diameter from almost 40 to about 100 nm. The extremely thin sections of these grains indicate overlap between the grains in some regions of the sample. The encompassing nature of the fine structure phase around the crystals seems to indicate that crystallization is occurring from within this fine structured region.

Upon increasing the heat treatment time to 4 h, the crystallized grains start to exhibit a more well-defined hexagonal shape as is observed in Fig. 6c. At this stage, the grain size is increased, with some of the grains varying between about 70–100 nm and in some cases even larger than 100 nm. Also, the extent of the very fine structured regions is significantly reduced, due to possible coalescence with the crystallized grain of hydroxyapatite. A selective area electron diffraction image (SAED) of a grain from the sample heat treated under these parameters is seen in Fig. 6d. The diffraction analysis indicated that the *d*-spacing between the spots was approximately 0.81 nm, which was consistent with *d*-spacings of the (100) planes of the hydroxyapatite unit cell. This was corroborated by the image observed in Fig. 6e. This image shows Moiré fringes caused by diffraction of the electron beam by two overlapping crystalline hydroyxapatite grains. The spacing between the lattice fringes corresponds to the spacing between the planes causing the electron beam diffraction. In this

(a)

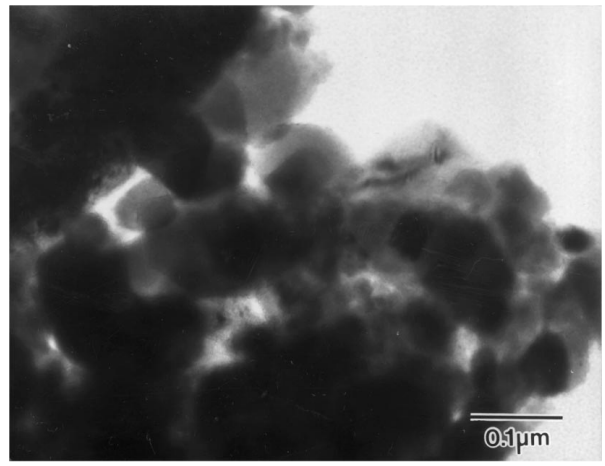

(b)

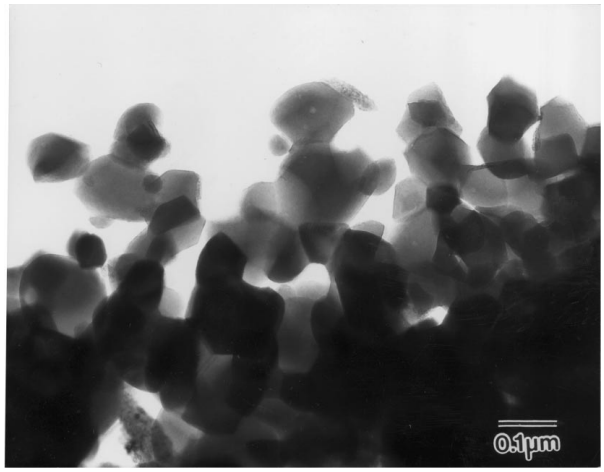

(c)

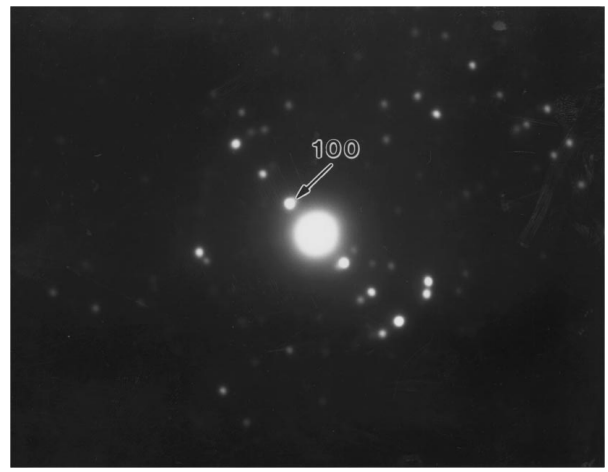

(d)

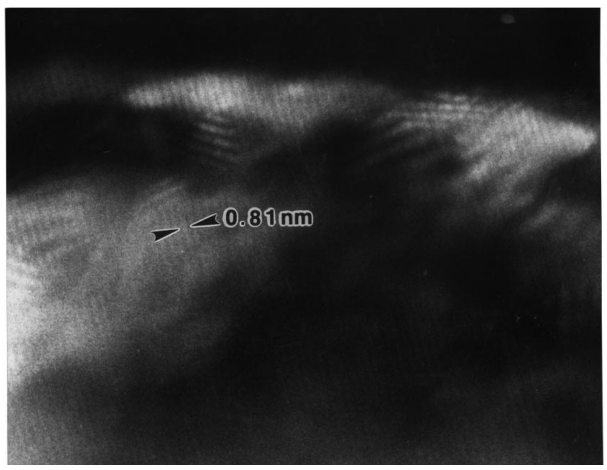

(e)

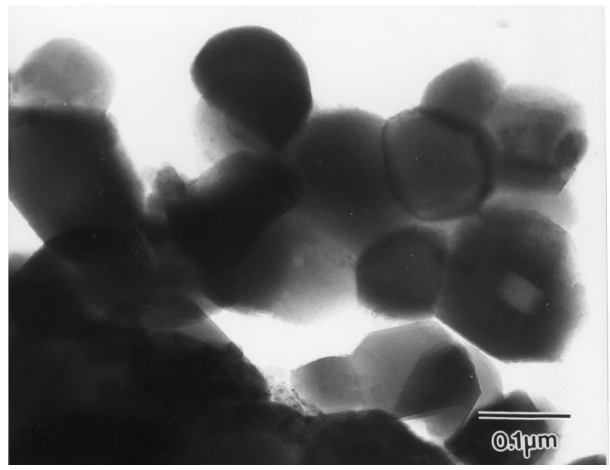

(f)

Figure 6 (a) TEM image of gel heat treated at 950 °C for 0.5 h, post HCl treatment, (b) TEM image of gel heat treated at 950 °C for 1 h, post HCl treatment, (c) TEM image of gel heat treated at 950 °C for 4 h, post HCl treatment, (d) Selective area electron diffraction image a grain from gel heat treated at 950 °C for 4 h, post HCl treatment, (e) TEM image indicating Moiré fringes due to electron diffraction from overlapping grains in gel heat treated at 950 °C for 4 h, post HCl treatment, (f) TEM image of gel heat treated at 950 °C for 8 h, post HCl treatment, and (g) TEM image of gel heat treated at 900 °C for 8 h, post HCl treatment. (*Continued*)

case, the spacing of the fringes at 0.81 nm is consistent with the spacing of the (100) planes, which are observed as a X-ray diffraction peak at 10.82° two-theta angle.

An increase in the heat treatment time to 8 h gives the system adequate kinetics to permit further growth of the hydroxyapatite grains, as observed in Fig. 6f. Almost all of the grains observed in this image are about 100 nm in size. A comparison of the development of the hydroxyapatite phase at this stage with that developed in a sample treated at 900 °C for 8 h shows similar crystallization of grains of the hydroxyapatite phase. However, much larger regions comprising of the fine structured material are also evident (see Fig. 6g). This can be explained by the fact that the crystallization and

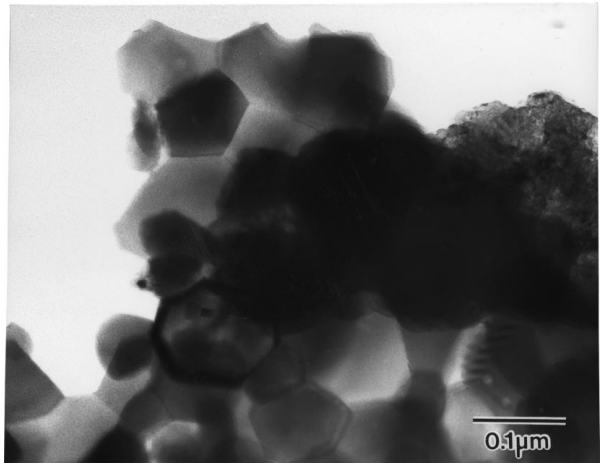

(g)

Figure 6 (*Continued*).

growth of the hydroxyapatite grains may be occurring at a slower rate due to the lower heat treatment temperature and hence, the remnants of the fine structured phase.

4. Conclusions

From electron microscopic studies involving the development of the hydroxyapatite phase processed by a sol-gel route, one observes the formation of visually distinguishable hydroxyapatite grains at temperature greater than 900 °C, though thermal analysis indicates crystallization of this phase at lower temperatures. An increase in the observable number and size of hydroxyapatite grains at about 900 °C may be aided by the increased amounts of thermal energy available at higher temperatures. The formation of hydroxyapatite is seen to occur by a process involving the nucleation of hydroxyapatite crystals from a very fine structured matrix, followed by the subsequent growth of these crystals with increasing exposure to high treatment temperatures. As the crystallization proceeds, the fine structured matrix is consumed leading one to believe that this matrix is a calcium phosphate matrix. The grains formed at lower temperatures do not exhibit a preferred growth habit, but grow in an equiaxed manner. At temperatures of about 1000 °C, the hydroxyapatite grains appear to develop a pronounced hexagonal shape. These grains form dense clusters in which triple points due to grain boundary junctions are well evident. At 1200 °C, the grains undergo exaggerated grain growth exhibiting a very pronounced hexagonal growth morphology consistent with the hexagonal unit cell in which hydroxyapatite crystallizes. Proof about the grains being predominantly hydroxyapatite is seen from the electron diffraction patterns and the Moiré fringes formed due to diffraction by the (100) planes with a d-spacing of 0.81 nm unique to hydroxyapatite. These planes are absent or do not give rise to detectable reflection in other apatite structures like the carbonate-hydroxyl apatite.

References

1. A. RAVGLIOLI and A. KRAJEWSKI, "Bioceramics: Materials, Properties, Application" (Chapman and Hall, London, 1992) p. 1.
2. L. L. HENCH, *J. Amer. Ceram. Soc.* **74** (1981) 1487.
3. R. H. DOREMUS, *J. Mater. Sci. Mater. in Med.* **27** (1992) 285.
4. P. DUCHEYENE, L. L. HENCH, A. KAGANII, M. MARTENS, A. BURSENS and J. C. MULIER, *J. Biomed. Mater. Res.* **14** (1980) 225.
5. S. D. COOK, J. F. KAY, K. A. THOMAS and M. JARCHO, *J. Oral Maxillof. Implants* **2** (1987) 15.
6. P. FRAYSSINET, F. TOURENNE, N. ROUQUET, P. CONTE, C. DELGA and G. BONEL, *J. Mater. Sci.: Mater. in Med.* **5** (1994) 11.
7. M. WEINLAENDER, J. BEUMER III, E. B. KENNEY, P. K. MOY and F. ADAR, *ibid.* **3** (1992) 397.
8. R. L. REIS and J. MONTEIRO, *ibid.* **7** (1996) 407.
9. E. G. NORDSTROM, L. NIEMI and J. MIETTINEN, *Biomed. Mater. and Eng.* **2** (1992) 115.
10. J. F. OSBORN and H. NEWESELY, *Biomaterials* **1** (1980) 108.
11. S. R. LEVITT, P. H. CRAYTON, E. A. MONROE and R. A. CONDRATE, *J. Biomed. Mater. Res.* **3** (1969) 683.
12. J. J. P. VALDES, A. V. RODRIGUEZ and J. G. CARRIO, *J. Mater. Res.* **10** (1995) 2174.
13. M. JARCHO, C. H. BOLEN, M. B. THOMAS, J. BOBICK, J. F. KAY and R. H. DOREMUS, *J. Mater. Sci.* **11** (1976) 2027.
14. P. W. BROWN, *J. Amer. Ceram. Soc.* **75** (1992) 17.
15. A. DEPTULA, W. LADA, T. OLCZAK, A. BORELLO, C. ALVANI and A. DI BARTOLOMEO, *J. Non-Cryst. Solids* **147/148** (1992) 537.
16. C. CHAI, B. BEN-NISSAN, S. PYKE and L. EVANS, *Mater. and Manuf. Processes* **10** (1995) 205.
17. D. B. HADDOW, P. F. JAMES and R. VAN NOORT, *J. Mater. Sci.: Mater. in Med.* **7** (1996) 255.
18. A. JILLAVENKATESA and R. A. CONDRATE, *J. Mater. Sci.* **33** (1997) 4111.

Received 30 October 1997
and accepted 9 March 1999